# Simultaneous Heat and Mass Transfer Accompanied by Phase Change in Porous Insulation

**K. Vafai**
Department of Mechanical Engineering,
Ohio State University,
Columbus, OH 43210
Mem. ASME

**S. Whitaker**
Department of Chemical Engineering,
University of California,
Davis, CA 95616

*This paper analyzes the accumulation and migration of moisture in an insulation material. The problem is modeled as a two-dimensional, transient, multiphase flow in a porous slab. The local volume-averaging technique is used to arrive at a rigorous and fundamental formulation of the heat and mass transfer process in an insulation system. The controlling parameters and assumptions are presented in detail. The equations are solved by devising a two-phase numerical scheme to obtain the condensation regions and the factors which affect the temperature distribution. The phase change process and its effects on the temperature, vapor density, moisture content, liquid content, and the vapor pressure distributions are discussed in detail. The significant transport mechanisms are identified and a simplified formulation of heat and mass transfer, accompanied by phase change, in an insulation system is presented.*

## 1 Introduction

Transport processes in porous media have been the subject of extensive investigations due to the applicability of such studies in a variety of problems, such as geothermal operations, soil hydrology, nuclear waste disposal, drying technology, and energy conservation. A very important area in the field of energy conservation is the effect of condensation on the performance of high-porosity insulation materials.

A typical insulation material consists of a solid matrix, a gas phase which itself consists of air and water vapor, and a very small amount of adsorbed liquid water. When the insulation matrix is exposed to environments of different temperature and humidity, diffusion and bulk convection of the air, vapor, and liquid occur. In addition, air infiltration due to small differences in total pressure across the insulation matrix augments this transport process. Condensation occurs at any point in the insulation where the water vapor concentration becomes greater than the saturation concentration corresponding to the temperature at that point. As the condensation takes place the latent heat of vaporization is released which acts as a heat source for the heat transfer process. The condensation also creates a liquid phase which may be pendular or mobile due to the capillary action and gravity. In summary, the complete problem is a combined mass, momentum, and energy transfer in a porous medium containing a multiphase mixture of air, vapor, and water in the void space. The general aspects of combined transport in porous media [1-7] are used in formulating and understanding the physics of condensation processes in the porous insulation.

It is crucial to gain a fundamental understanding of the conditions which promote condensation, as condensation will significantly affect energy transfer across the insulation matrix. This in turn greatly influences the $R$ value of the insulation. Furthermore, condensation directly affects the physical integrity of the insulation and its deterioration. A more thorough knowledge of the condensation process in an insulation material will allow better predictions of the condensation rates and the qualitative effects of the controlling parameters. In addition, an understanding of the condensation process will ultimately help in establishing the design locations for the vapor barriers.

Contributed by the Heat Transfer Division for publication in the JOURNAL OF HEAT TRANSFER. Manuscript received by the Heat Transfer Division May 9, 1984.

The analysis in this paper quantifies the process of moisture accumulation and presents a rigorous and fundamental formulation of heat and mass transfer, accompanied by phase change, in an insulation system. The pertinent variables in an insulation system are presented and the significant transport mechanisms are identified. The variations among the pertinent variables are thoroughly investigated for two types of basic step changes in the temperature and moisture content boundary and initial conditions. Finally, a simplified formulation of heat transfer, accompanied by phase change, in an insulation system is presented. This is done through a systematic investigation of the rigorous formulation to determine which mechanisms have a negligible effect on the pertinent variables.

## 2 Analysis

The formulation of the problem is based on using the local volume-averaging technique for mass, momentum, and energy equations for each phase to derive the governing equations for the condensation process in an insulation material. This is done by associating with every point in the porous medium a small volume $V$ bounded by a closed surface $A$. In general, the volume $V$ is composed of three phases. These are: the solid phase $V_\sigma$, the liquid phase $V_\beta(t)$, and the gas phase $V_\gamma(t)$. An intrinsic phase average for a quantity $\phi$ in phase $\alpha$ is defined as

$$<\Phi_\alpha>^\alpha = \frac{1}{V_\alpha(t)} \int_{V_\alpha(t)} \Phi_\alpha dV \tag{1}$$

where $\Phi_\alpha$ is a quantity associated with the $\alpha$ phase. Another quantity of interest is the spatial average for the quantity $\Phi$ which is defined as

$$<\Phi> = \frac{1}{V} \int_V \Phi \, dV \tag{2}$$

Several simplifying assumptions are made in order to obtain the governing equations for condensation in insulation materials:

I The total gas phase pressure in the insulation matrix is constant. This pressure is denoted by $p_{\text{total}}$.

II The insulation material is homogeneous and isotropic.

III The solid-liquid-gas system is in local thermal equilibrium.

IV The liquid and the gas mass flux vectors are in the

same direction. However, there are no restrictions on the magnitudes of the liquid and the gas mass flux vectors.

V The inert gas component in the insulation matrix, which is air, is stagnant. However, the vapor is mobile.

Assumptions I, II, and III are usually justified for an insulation material and assumption IV is physically appealing and justifiable. The simplifying assumption V places the emphasis on the condensation process. Assumption V allows both vapor and liquid phases to be mobile. The nondimensional governing equations, obtained after considerable algebraic manipulation of previous work [1-3] on drying, are given in dimensionless form as

Energy equation:

$$<\rho>C_p\frac{\partial<T>}{\partial t}-\Lambda\,\psi_s(\nabla S\cdot\nabla<T>)-\psi_T\Lambda(\nabla<T>\cdot\nabla<T>)+\Lambda\,\psi_g(\mathbf{g}\cdot\nabla<T>)+<\dot{m}>=\nabla\cdot(k_{\text{eff}}\nabla<T>) \tag{3}$$

Moisture transport equation:

$$\frac{\partial S}{\partial t}=\nabla\cdot(\psi_s\nabla S)+\nabla\cdot(\psi_T\nabla<T>)-\nabla\cdot(\psi_g\mathbf{g}) \tag{4}$$

Gas phase equation:

$$\frac{\partial(\epsilon_\gamma<\rho_v>^\gamma)}{\partial t}-\frac{<\dot{m}>}{P_4}=\psi_D\nabla^2<\rho_v>^\gamma \tag{5}$$

Volumetric constraint:

$$\epsilon_\sigma+\epsilon_\beta+\epsilon_\gamma=1 \tag{6}$$

Thermodynamic relations:

$$<p_a>^\gamma=p_{\text{total}}-<p_v>^\gamma \tag{7}$$

$$<p_a>^\gamma=P_{11}<\rho_a>^\gamma<T> \tag{8}$$

$$<p_v>^\gamma=P_8<\rho_v>^\gamma<T> \tag{9}$$

$$<p_v>^\gamma=\exp\left[-\frac{2P_9}{<T>}-P_{10}\left(\frac{1}{<T>}-\frac{1}{T_0}\right)\right] \tag{10}$$

where

$$\rho=\frac{\bar{\rho}}{\bar{\rho}_0},\ C_p=\frac{\bar{C}_p}{\bar{c}_0},\ T=\frac{\bar{T}}{\Delta\bar{T}},\ \rho_i=\frac{\bar{\rho}_i}{\bar{\rho}_0},\ k_i=\frac{\bar{k}_i}{\bar{k}_{0,\text{eff}}} \tag{11}$$

$$p_i=\frac{\bar{p}_i}{\bar{p}_{v,0}},\ x_i=\frac{\bar{x}_i}{\bar{L}},\ c_i=\frac{\bar{c}_i}{\bar{c}_0} \tag{12}$$

$$k_{\text{eff}}=\frac{\bar{k}_{\text{eff}}}{\bar{k}_{0,\text{eff}}},\ t=\frac{\bar{t}}{\bar{L}^2/\bar{\alpha}_{0,\text{eff}}},\ \mathbf{g}=\frac{\bar{\mathbf{g}}}{\bar{g}_0},\ \dot{m}=\frac{\bar{\dot{m}}}{\bar{\rho}_0\bar{c}_0\Delta\bar{T}\,\bar{\alpha}_{0,\text{eff}}/\bar{L}^2\Delta\bar{h}_{\text{vap}}} \tag{13}$$

$$\psi_s=\frac{\bar{D}}{\bar{\alpha}_{0,\text{eff}}},\ \psi_D=\bar{D}_{v,\text{eff}}/\bar{\alpha}_{0,\text{eff}},\ \alpha_{0,\text{eff}}=\frac{\bar{k}_{0,\text{eff}}}{\bar{\rho}_0\bar{c}_0} \tag{14}$$

## Nomenclature

$C_p$ = dimensionless mass fraction averaged heat capacity = $\bar{C}_p/\bar{c}_0$

$\bar{c}_i$ = dimensional heat capacity at constant pressure for phase $i$, Ws/kgK

$\bar{c}_0$ = dimensional reference heat capacity at constant pressure, Ws/kgK

$\bar{D}$ = moisture transport coefficient, $m^2/s$

$\bar{D}_{v,\text{eff}}$ = vapor effective diffusivity coefficient, $m^2/s$

$\mathbf{g}$ = dimensionless gravity vector

$\Delta\bar{h}_{\text{vap}}$ = enthalpy of vaporization per unit mass, J/kg

$\bar{k}_i$ = dimensional thermal conductivity for phase $i$, W/mK

$\bar{k}_T$ = a parameter which is related to the gradient of the capillary pressure with respect to temperature, $kg/ms^2K$

$k_{\text{eff}}$ = dimensionless effective thermal conductivity = $\bar{k}_{\text{eff}}/\bar{k}_{0,\text{eff}}$

$\bar{K}_\beta$ = liquid phase permeability, $m^2$

$\bar{L}$ = characteristic length of the insulation, m

Le = Lewis number = $\alpha_{0,\text{eff}}/\bar{D}$

$\dot{m}$ = dimensionless condensation rate = $\bar{\dot{m}}/[\bar{\rho}_0\bar{c}_0(\bar{T}_H-\bar{T}_C)\,\bar{\alpha}_{0,\text{eff}}/\bar{L}^2\Delta\bar{h}_{\text{vap}}]$

$p_{\text{total}}$ = dimensionless total pressure in the enclosure = $\bar{p}_{\text{total}}/\bar{p}_{v,0}$

$\bar{R}_a$ = air gas constant, Nm/kgK

$\bar{R}_v$ = vapor gas constant, Nm/kgK

$S$ = the moisture content, defined in equation (17)

$t$ = dimensionless time = $\bar{t}/(\bar{L}^2/\bar{\alpha}_{0,\text{eff}})$

$T$ = dimensionless temperature = $\bar{T}/(\bar{T}_H-\bar{T}_C)$

$\bar{T}_H$ = reference temperature for the hot side of the insulation, K

$\bar{T}_C$ = reference temperature for the cold side of the insulation, K

$\bar{\alpha}_{0,\text{eff}}$ = reference effective thermal diffusivity = $\bar{k}_{0,\text{eff}}/\bar{\rho}_0\bar{c}_0$, $m^2/s$

$\epsilon$ = volume fraction

$\zeta$ = the ratio of the magnitudes of the gas phase to the total mass flux, defined in equation (18)

$\bar{\mu}_\beta$ = liquid dynamic viscosity, kg/ms

$\rho$ = dimensionless total density = $\bar{\rho}/\rho_0$

$\rho_v$ = dimensionless vapor density = $\bar{\rho}_v/\bar{\rho}_0$

$\bar{\rho}_i$ = dimensional density for phase $i$, $kg/m^3$

$\bar{\sigma}_{\beta\gamma}$ = surface tension at the vapor and gas interface, N/m

$\psi_i$ = denotes different thermophysical properties of the insulation system, defined in equations (14)-(16)

### Subscripts, Superscripts, and Symbols

$a$ = air phase

$D$ = reference to the parameter $\psi_D$, defined in equation (14)

eff = effective properties

$g$ = reference to the parameter $\psi_g$, defined in equation (16)

$i$ = $i$th phase

0 = reference quantities

$s$ = reference to the parameter $\psi_s$, defined in equation (14)

$T$ = reference to the parameter $\psi_T$, defined in equation (15)

$v$ = vapor phase

vap = vaporization

$\alpha$ = $\alpha$ phase

$\beta$ = liquid phase

$\gamma$ = gas phase

$\sigma$ = solid phase

$\bar{}$ = dimensional quantities

$< >$ = "local volume average" of a quantity

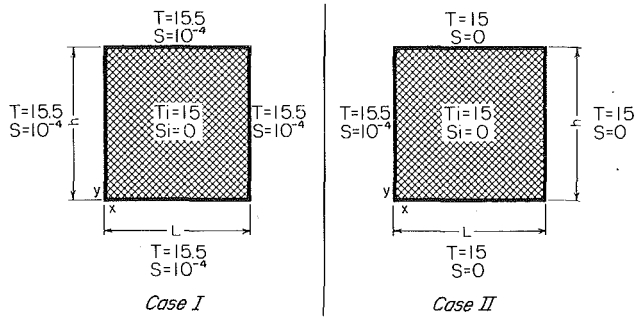


**Fig. 1 Transient condensation in an insulation slab for two different cases**

$$\psi_T = \frac{\epsilon_\beta \bar{K}_\beta \nabla \bar{T} \bar{k}_T}{\bar{\alpha}_{0,\text{eff}}(\epsilon_\beta + \epsilon_\gamma)\bar{\mu}_\beta} \tag{15}$$

$$\psi_g = \frac{\epsilon_\beta (\bar{\rho}_\beta - \bar{\rho}_\gamma)\bar{K}_\beta \bar{L}\, \bar{g}_0}{\bar{\alpha}_{0,\text{eff}}\bar{\mu}_\beta(\epsilon_\beta + \epsilon_\gamma)} \tag{16}$$

$$S = (\epsilon_\beta P_1 + \epsilon_\gamma <\rho_v>^\gamma)/P_1(\epsilon_\beta + \epsilon_\gamma) \tag{17}$$

$$\zeta = \frac{(\psi_D)\,|\nabla <\rho_v>^\gamma|}{P_1(\epsilon_\beta + \epsilon_\gamma)\,|\psi_s \nabla S + \psi_T \nabla <T> - \psi_g \bar{g}|} \tag{18}$$

$$\Lambda = P_1[P_2(1-\zeta) + P_3\zeta](\epsilon_\beta + \epsilon_\gamma) \tag{19}$$

$$\Delta\bar{T} = \bar{T}_H - \bar{T}_C$$

$$<\rho> = \epsilon_\sigma \rho_\sigma + \epsilon_\beta \rho_\beta + \epsilon_\gamma (<\rho_v>^\gamma + <\rho_a>^\gamma) \tag{20}$$

$$C_p = \frac{\epsilon_\sigma \rho_\sigma c_\sigma + \epsilon_\beta \rho_\beta c_\beta + \epsilon_\gamma (c_v <\rho_v>^\gamma + c_a <\rho_a>^\gamma)}{<\rho>} \tag{21}$$

$$k_{\text{eff}} \cong \epsilon_\sigma k_\sigma + \epsilon_\beta k_\beta + \epsilon_\gamma \frac{(k_v <\rho_v>^\gamma + k_a <\rho_a>^\gamma)}{<\rho_v>^\gamma + <\rho_a>^\gamma} \tag{22}$$

and

$$P_1 = \frac{\bar{\rho}_\beta}{\bar{\rho}_0},\ P_2 = \frac{\bar{c}_\beta}{\bar{c}_0},\ P_3 = \frac{\bar{c}_\gamma}{\bar{c}_0},\ P_4 = \frac{\Delta\bar{h}_{v\&p}}{\bar{c}_0 \Delta\bar{T}} \tag{23}$$

$$P_8 = \frac{\Delta\bar{T}\,\bar{R}_v \bar{\rho}_0}{\bar{P}_{v,0}},\ P_9 = \frac{\bar{\sigma}_{\beta\gamma}}{\bar{r}_0 \bar{\rho}_\beta \bar{R}_v \Delta\bar{T}} \tag{24}$$

$$P_{10} = \frac{\Delta\bar{h}_{\text{vap}}}{\bar{R}_v \Delta\bar{T}},\ P_{11} = \frac{\Delta\bar{T}\,\bar{R}_a \bar{\rho}_0}{\bar{P}_{v,0}} \tag{25}$$

Based on the above equations the primary variables for porous insulation are: $T$, the temperature; $S$, the moisture content; $\rho_v$, the vapor density; $p_v$, the vapor pressure; $\epsilon_\beta$, the liquid volume fraction; and $\epsilon_\gamma$, the gaseous volume fraction. The quantities with a subscript "0" refer to the reference quantities, and the variables with a bar on top refer to dimensional quantities.

The boundary conditions for these equations are considered in detail in the next section. In developing the governing equations it is assumed that the moisture transport coefficient $D$ is a constant. However, without any available experimental data, the moisture transport coefficient is not a known quantity. Therefore, experimental investigations are needed in this area. The value of $D$ which was used in this analysis was $4 \times 10^{-5}$ m$^2$/s. This value is based on the fact that the moisture transport coefficient is dominated by the gas phase diffusion for very small values of the liquid content.

In analyzing the heat and mass transfer process in porous insulation the following physical data were used in the numerical computations: $\bar{L} = 0.12$ m, $\epsilon_\sigma = 0.03$, $\bar{T}_H = 313$ K, $\bar{T}_c = 293$ K, $\bar{\rho}_0 = 32$ kg/m$^3$, $\bar{c}_0 = 842$ Ws/kgK, $\bar{\sigma}_{\beta\gamma} = 0.073$ kg/s$^2$, and $K_\beta = 10^{-10}$ m$^2$. These data correspond to a typical fibrous insulation material.

## 3 Transient Condensation in an Insulation Slab

To analyze the significance of the condensation problem in an insulation material, two different cases are considered. These cases are shown in Fig. 1. In Case I the entire periphery of the slab is suddenly subjected to a different temperature and moisture content and in Case II only one surface of the slab is subjected to a different temperature and moisture content.

In both cases the transient behavior for all of the pertinent variables is analyzed and a sample of the results is presented. The specific boundary and initial conditions which were used for Cases I and II were:

Case I

$$\begin{aligned} T(x=0,\ L;\ y;\ t) &= 15.5 \\ T(x;\ y=0,\ h;\ t) &= 15.5 \\ S(x=0,\ L;\ y;\ t) &= 10^{-4} \\ S(x;\ y=0,\ h;\ t) &= 10^{-4} \end{aligned} \tag{26}$$

Initial conditions:

$$\begin{aligned} T(x;\ y;\ t=0) &= 15 \\ S(x;\ y;\ t=0) &= 0 \end{aligned}$$

Case II

$$\begin{aligned} T(x=0;\ y;\ t) &= 15.5 \\ T(x=L;\ y;\ t) &= 15 \\ T(x;\ y=0,\ h;\ t) &= 15 \\ S(x=0;\ y;\ t) &= 10^{-4} \\ S(x=L;\ y;\ t) &= 0 \\ S(x;\ y=0,\ h;\ t) &= 0 \end{aligned} \tag{27}$$

Initial conditions:

$$\begin{aligned} T(x;\ y;\ t=0) &= 15 \\ S(x;\ y;\ t=0) &= 0 \end{aligned}$$

The dimensionless temperature at the boundary is chosen to correspond to a hot and humid environment on the outside and a colder environment inside of the insulation slab.

One of the objectives of this investigation is to show how the pertinent variables vary with respect to each other for the two types of basic step changes in moisture content and temperature boundary conditions given in equations (26) and (27). These two cases provide two kinds of fundamental step changes in the temperature and humidity of the environment surrounding an insulation slab.

To analyze the above two cases, equations (3) to (10) were solved subject to boundary conditions (26) and (27). The nine unknowns in these equations are: $<T>$, $S$, $<\dot{m}>$, $<\rho_v>^\gamma$, $<p_v>^\gamma$, $<\rho_a>^\gamma$, $<p_a>^\gamma$, $\epsilon_\beta$, and $\epsilon_\gamma$. The nine equations which will uniquely define these unknowns are equations (3) to (10) plus equation (17). These equations were solved using an upwind differencing scheme for the convective terms. The upward differencing was possible since the analysis provided an explicit expression for the direction of the liquid and vapor velocities.

## 4 Two-Phase Format Numerical Scheme

Initially the insulation slab was assumed to be composed of a solid matrix, water vapor, and air. That is

$$\epsilon_\beta = 0 \qquad \text{at } t = 0 \tag{28}$$

Although this condition could be relaxed very easily, this

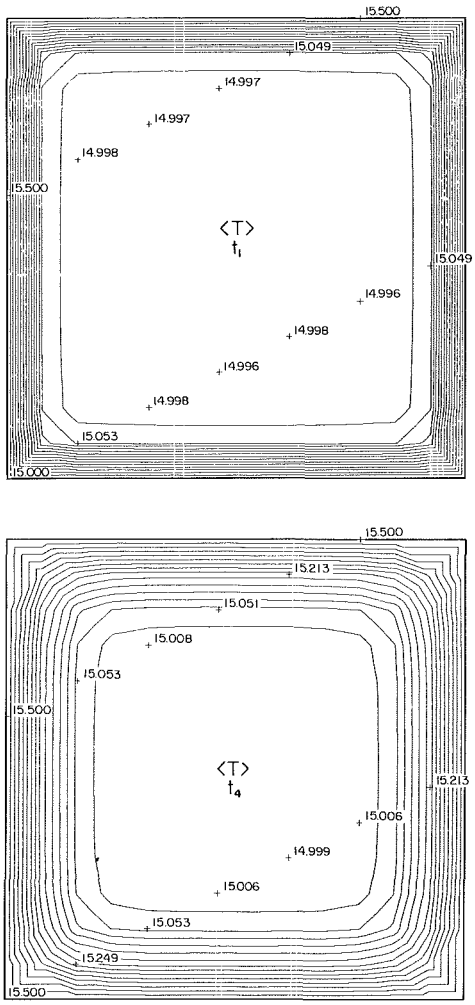


**Fig. 2 Spatial variation of temperature inside the insulation slab at two different times (Case I): $t_1 = 2.3 \times 10^{-3}$, $t_4 = 1.4 \times 10^{-2}$**

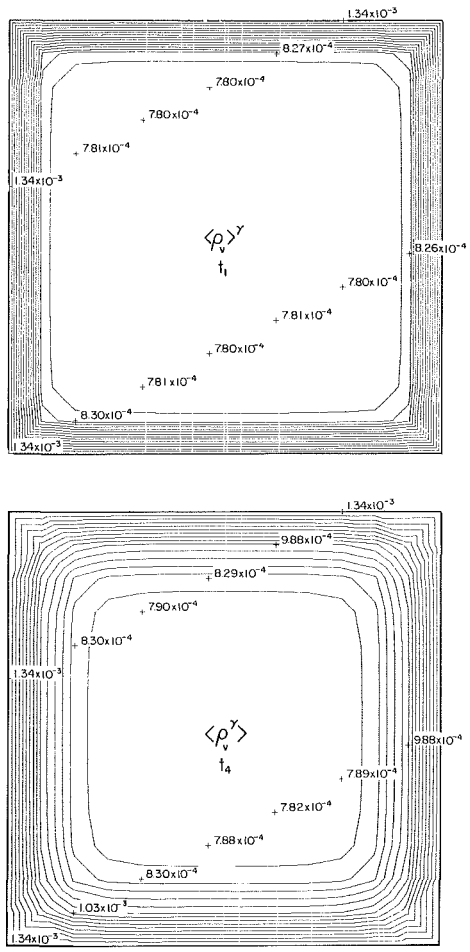


**Fig. 3 Vapor density contours at two different times corresponding to Fig. 2 (Case I)**

choice was considered to correspond to a more fundamental situation. With no liquid present in the insulation matrix the value of $\zeta$, which is the ratio of the gas phase to the total mass flux, becomes:

$$\zeta = 1 \qquad \text{at } t = 0 \tag{29}$$

In addition, due to the large value of the liquid density compared to the vapor density, the moisture content inside of the slab becomes approximately zero, i.e.

$$S = 0 \qquad \text{at } t = 0 \tag{30}$$

It should be noted that the boundary conditions on the moisture content and the temperature are given by equations (26) and (27). These were discussed in the previous section. At the beginning of the condensation process an appropriate condition for the condensation rate is:

$$<\dot{m}> = 0 \qquad \text{at } t = 0 \tag{31}$$

Based on the experimental results of Langlais et al. [8] values of $\epsilon_\beta < 10^{-6}$ were considered to be part of the adsorbed water. Therefore, at any time and location in the slab for which $\epsilon_\beta$ was less than $10^{-6}$, the condensation rate was set equal to zero. For $\epsilon_\beta > 10^{-6}$, again based on Langlais' data [8], condensation was assumed to have actually occurred. Equation (10) was used and the condensation rate $<\dot{m}>$ was found from the governing equations. Starting with the initial values of the temperature and moisture content, equations (3) to (10) were solved by two different formats depending on the value of $\epsilon_\beta$. These were:

*Format I.* This format was followed for any time and location in space for which $\epsilon_\beta < 10^{-6}$.

1 Initial values of $<\rho_v>^\gamma$, $<p_v>^\gamma$, $<p_a>^\gamma$, and $<\rho_a>^\gamma$ were obtained from equations (17), (9), (7), and (8). (Step 1 was applied only at the initial time step $t = 0$.)

2 $<\dot{m}>$ was set equal to zero as discussed above.

3 $<\rho_v>^\gamma$ was obtained from the gas phase equation (5).

4 $S$ and $<T>$ were obtained from equations (3) and (4).

5 $\epsilon_\beta$ and $\epsilon_\gamma$ were obtained from equation (17) and the volumetric constraint.

6 The $\zeta$ distribution was obtained from equation (18).

7 $<p_v>^\gamma$, $<p_a>^\gamma$, and $<\rho_a>^\gamma$ were obtained from the thermodynamic relations.

8 $<p_v>^\gamma$ and $<\rho_v>^\gamma$ were solved for from equations (10) and (9), respectively.

9 If, at any location, the $<\rho_v>^\gamma$ obtained in step 3 was greater than or equal to the one obtained in step 8, then Format II was adopted for the next time step at that location.

*Format II.* This format was followed for any time and location in space for which $\epsilon_\beta > 10^{-6}$.

1 $<p_v>^\gamma$, $<\rho_v>^\gamma$, $<p_a>^\gamma$, $<\rho_a>^\gamma$, and $\epsilon_\gamma$ were obtained from the thermodynamic relations and the volumetric constraint. (Step 1 was applied only at the initial time step $t = 0$.)

2 The moisture content distribution was obtained from equation (4).

3 The temperature distribution was obtained from equation (3).

4 The new moisture content and temperature distributions

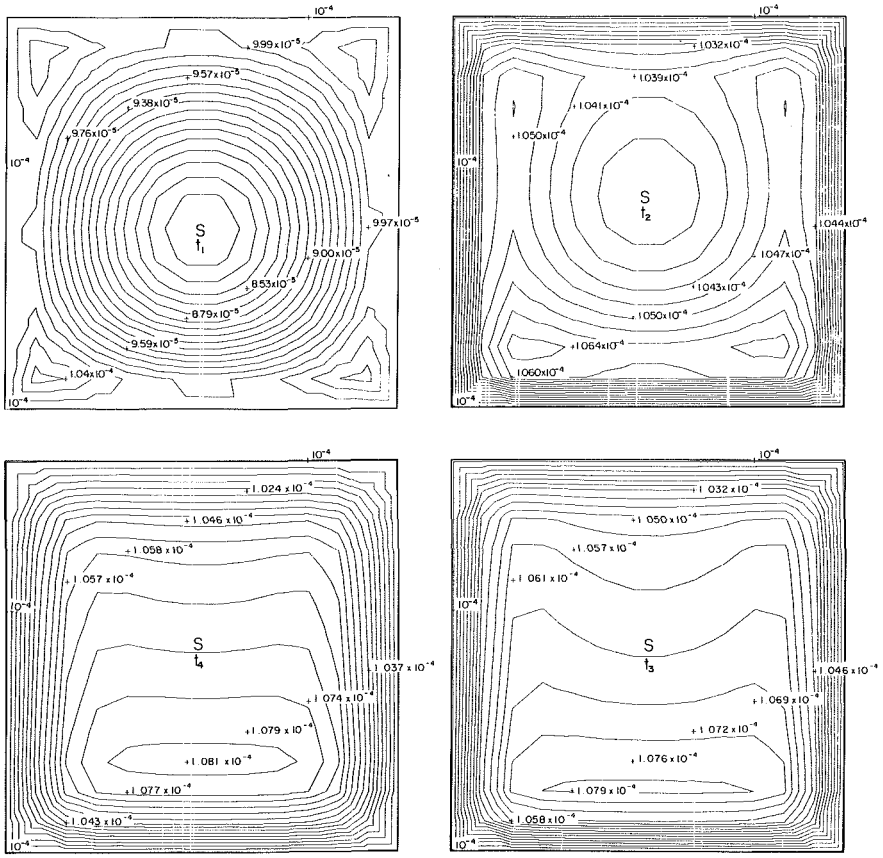


**Fig. 4 Spatial variation of the moisture content inside the insulation slab at four different times corresponding to Fig. 2 (Case I)**

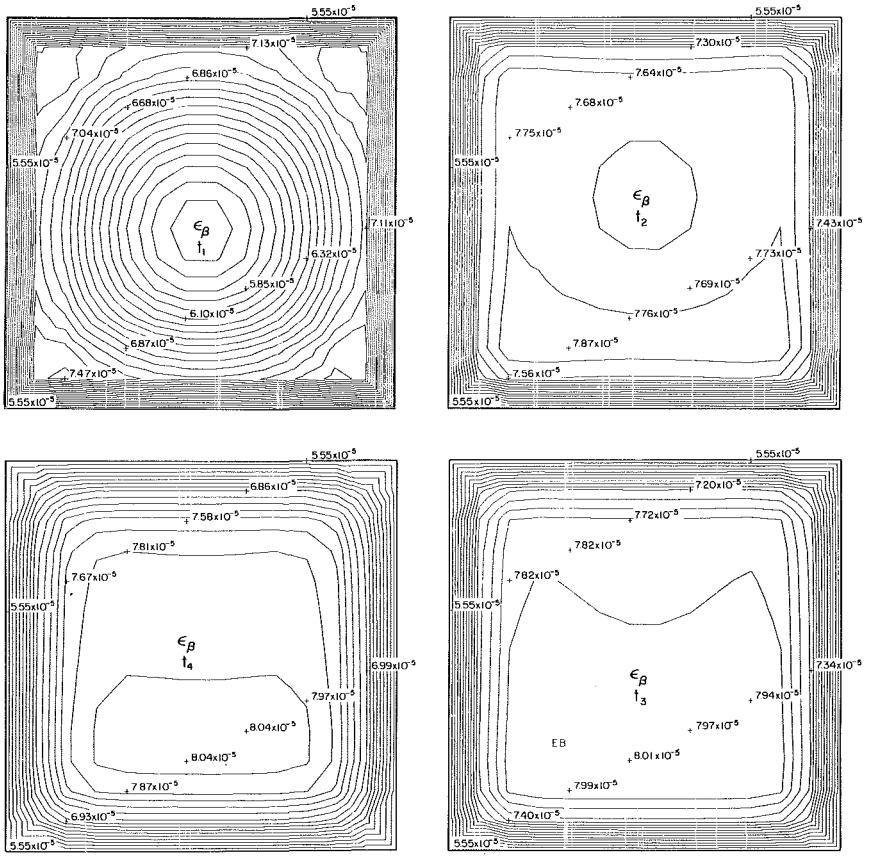


**Fig. 5 Liquid fraction contours at four different times corresponding to Fig. 2 (Case I)**

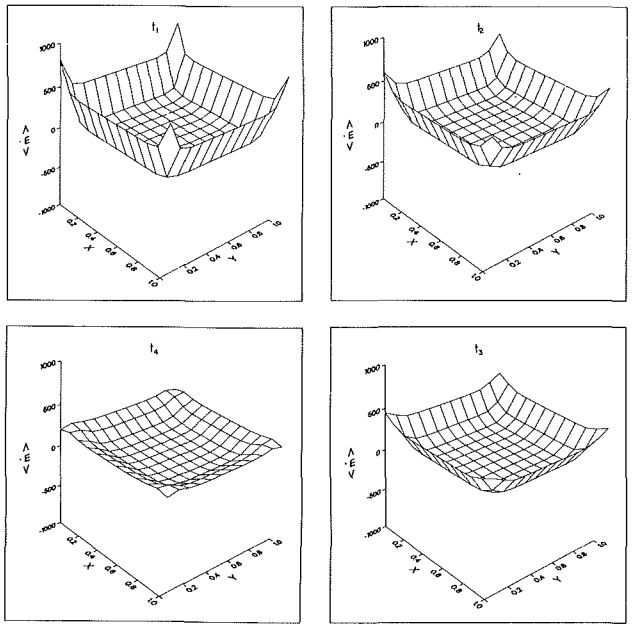

Fig. 6 Three-dimensional condensation and evaporation rate plots at four different times corresponding to Fig. 2 (Case I)

were used to find the distributions for $<p_v>^{\gamma}$, $<\rho_v>^{\gamma}$, $<p_a>^{\gamma}$, $<\rho_a>^{\gamma}$, $\epsilon_{\gamma}$, and $\epsilon_{\beta}$ from the thermodynamic relations, the volumetric constraint, and equation (17).

5 The $\zeta$ distribution was obtained from equation (18).

6 The condensation rate was obtained from equation (5).

To the authors' knowledge this two-dimensional computational analysis, which accounts for the phase change process, is presented for the first time.

## 5 Discussion of Results and Conclusions

Results are presented for a square fibrous insulation slab. The pertinent variables for both cases are the temperature, moisture content, liquid fraction, vapor density, and the condensation rate. Figures 2–6 present the spatial variations of these quantities for Case I at several different times. Crosses are marked at every $m + 2$ (where $m$ is the number of grid points in the $x$ direction) node in the numerical mesh system. Corresponding values are printed to the right of each cross. Figures 4, 5, and 6 demonstrate some significant changes which occur in the growth characteristics of $S$, $\epsilon_{\beta}$, and $<\dot{m}>$. The times $t_1$, $t_2$, $t_3$, and $t_4$ were chosen to reflect these significant changes. However, there are no significant changes in the growth characteristics of $<T>$ and $<\rho_v>^{\gamma}$ at times $t_2$ and $t_3$. These variables are therefore presented only at times $t_1$ and $t_4$.

As expected, the interior temperature of the slab increases with time when the boundary temperature is suddenly increased, as can be seen in Fig. 2. This rise in temperature is the result of simultaneous diffusion and convection of heat from the boundary as well as moisture condensation. Condensation acts as a source of local heat generation and evaporation acts as an energy sink. The increase in temperature starts at regions close to the exterior boundary and gradually moves inward. This wavelike propagation is also observed for $S$, $\epsilon_{\beta}$, $<\rho_v>^{\gamma}$, and $<\dot{m}>$. In the three-dimensional plot (Fig. 6) the condensation regions have a positive value of $<\dot{m}>$ and the evaporation regions have a negative value of $<\dot{m}>$.

In the beginning, as condensation occurs, the liquid and moisture contents increase in the regions close to the external boundary where the temperature is close to the initial interior temperature. As the temperature close to the external boundary increases with time the liquid and moisture content

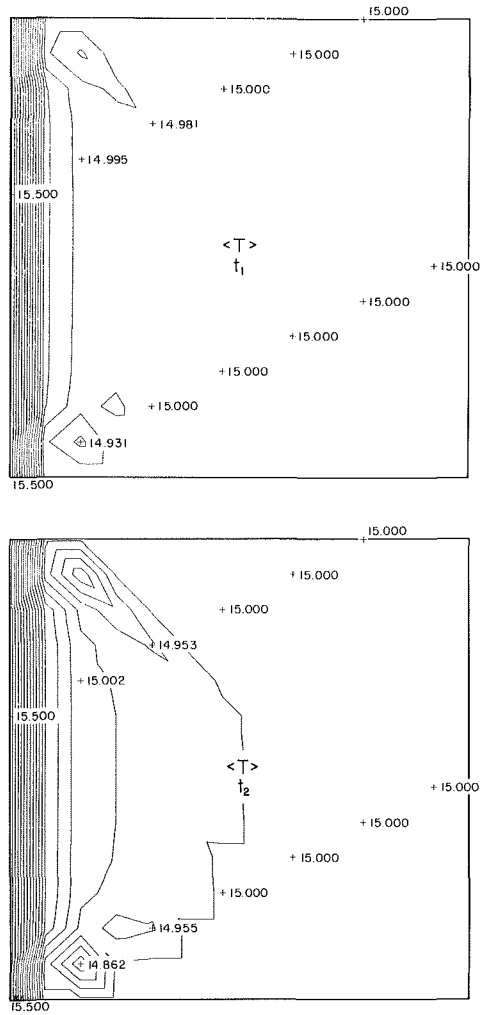


Fig. 7 Spatial variation of temperature inside the insulation slab at two different times (Case II): $t_1 = 2.3 \times 10^{-3}$, $t_2 = 4.6 \times 10^{-3}$

should decrease in that region. However, in the regions away from the immediate external boundary, where the temperature has not increased or has increased only slightly, the liquid and moisture contents should increase. These trends can be seen in Figs. 2–6. Also seen in Figs. 2–6 are regions of mild evaporation. The evaporation leads to a drop in temperature in those regions.

One of the important parameters which affects this relative movement of the temperature wavefront compared to the liquid and the moisture wavefronts is the ratio of the effective thermal diffusivity to the moisture transport coefficient. This ratio, which is known as the Lewis number Le, also affects the liquid content inside the insulation slab. Increasing the Lewis number decreases $\epsilon_{\beta}$ at a given time and position, and decreasing Le increases $\epsilon_{\beta}$ at a given time and position.

In the regions where condensation occurs, the temperature inside the slab increases continuously causing the vapor pressure to increase. This is expected from equation (10), since $p_{10} \gg p_9$. Consequently the vapor density increases with time. This is because $<\rho_v>^{\gamma} = <p_v>^{\gamma}/P_8 <T>$ and although $1/<T>$ decreases as $<T>$ increases, the increase in $<p_v>^{\gamma}$ with an increase in $<T>$ not only offsets the decrease in $1/<T>$ but it results in a net increase in $<\rho_v>^{\gamma}$ with temperature. This behavior can be observed in Fig. 3. In the above calculations it is assumed that the liquid content has not deteriorated the structural integrity of the porous matrix. This is a reasonable assumption to make for small amounts of liquid content, as is the case here. It should also be noted that

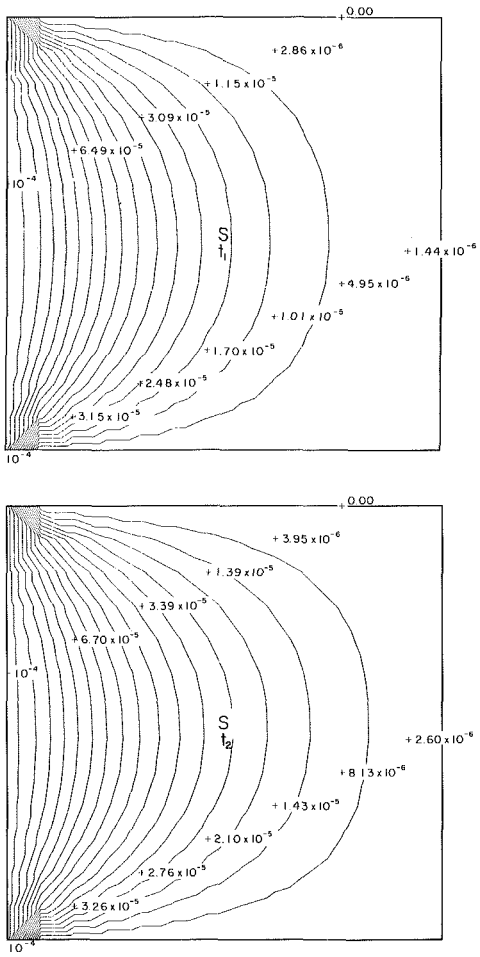


**Fig. 8 Spatial variation of the moisture content inside the insulation slab at two different times corresponding to Fig. 7 (Case II)**

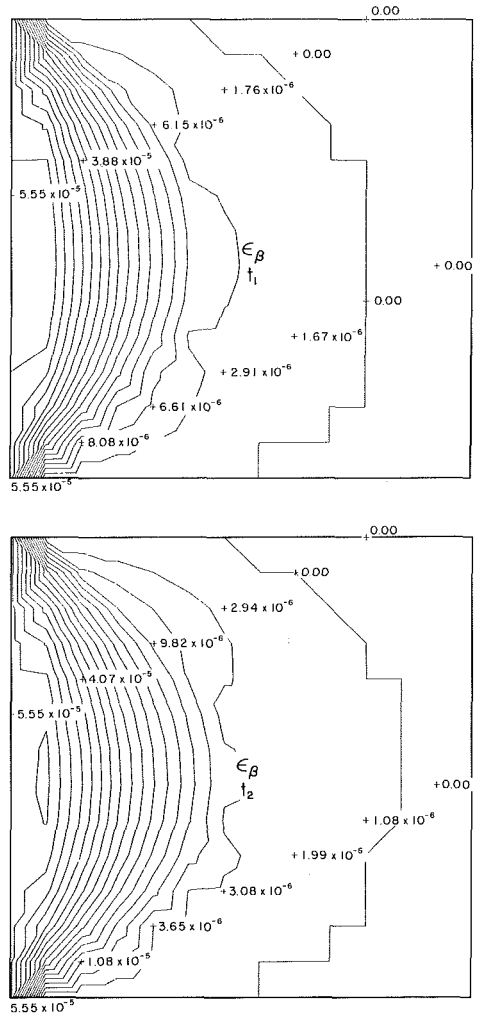


**Fig. 9 Liquid fraction contours at two different times corresponding to Fig. 7 (Case II)**

a larger liquid fraction is created at the bottom of the insulation slab, due to the gravity forces, as seen in Figs. 4 and 5.

Figures 7–10 present the results of Case II for $<T>$, $S$, $\epsilon_\beta$, and $<\rho_v>^\gamma$ at two different times. It can be seen that the discussion used to describe the behavior of temperature, liquid fraction, and condensation rate for Case I also prevails here. The wavelike propagation of information from the left-hand boundary is clearly displayed in these figures. The propagation of the condensation front from the left side of the insulation slab as well as the regions where condensation and evaporation occur are displayed in three dimensions in Fig. 11 at four different times. Again a drop in temperature is observed in the evaporation regions. Condensation distorts the temperature distribution significantly. The temperature distribution changes very little from the initial condition when there is no condensation for the two times shown in Fig. 7. This is due to the very low conductivities of fibrous insulation and vapor and the absence of any phase change.

The physics and the accuracy of the numerical solution were tested in four different ways. First, it was observed that for the case of zero gravity, all of the variables should be symmetric with respect to the center of the insulation slab. This was indeed the situation for all of the cases which were tested. Figure 12 presents the moisture and liquid content contour plots for Case I when the gravitational forces are neglected.

Second, it is expected that for longer times the variables $<T>$, $\epsilon_\beta$, $\epsilon_\gamma$, $<p_v>^\gamma$, $<\rho_v>^\gamma$, and $S$, inside of the slab, become uniform and approach the values at the periphery of the slab. Furthermore the condensation rate should approach zero due to the uniform temperature inside of the slab. This was tested and confirmed for a number of different situations. Figure 13 presents the temperature and the vapor pressure contours at two later times for Case I. Figure 14 presents the three-dimensional condensation rate plots corresponding to Fig. 13. It is clear from Fig. 14 that the condensation rate does approach zero as it should.

Third, the accuracy of the numerical scheme was checked by increasing the number of grid points and the number of time steps. An increase in the number of grid points requires an increase in the number of time steps and a large increase in the time required to run the program. This is due to the large number of variables which have to be processed simultaneously. It was observed that although an increase in the number of grid points increased the quality of the contour lines (making them much smoother), it did not significantly alter the qualitative features of the contour plots. Therefore, to conserve the computer time and expense, a grid size of 15 $\times$ 15 was used.

Fourth, for no condensation and no convection, the numerical results are expected to reduce to a conduction case. This was observed by the numerical results.

From numerous numerical computations it is found that in general:

I The direct coupling between the moisture content $S$ and the temperature $<T>$ in the energy equation is weak. Therefore the term representing this coupling,

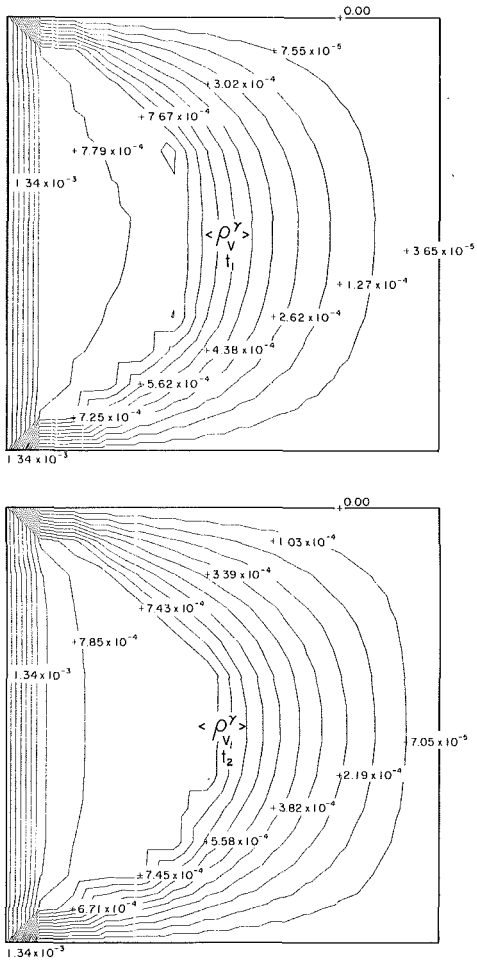


Fig. 10 Vapor density contours at two different times corresponding to Fig. 7 (Case II)

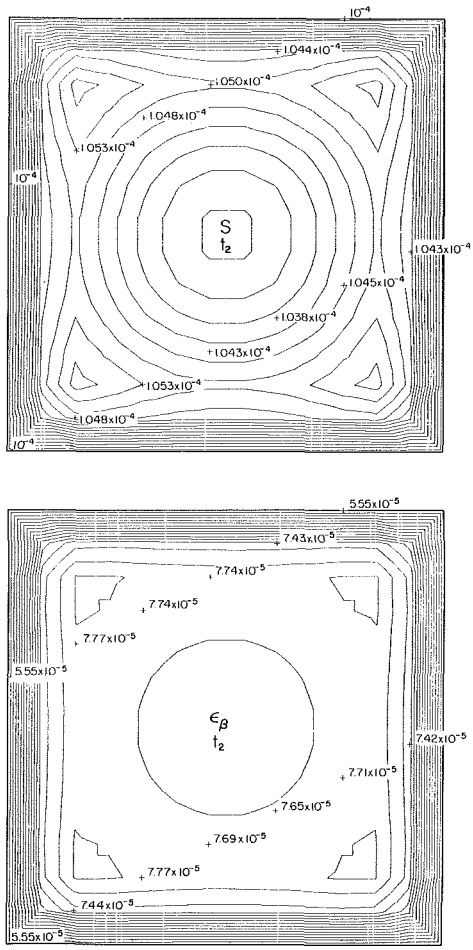


Fig. 12 Moisture and liquid fraction at $t_2 = 4.6 \times 10^{-3}$ when the gravitational effects are neglected

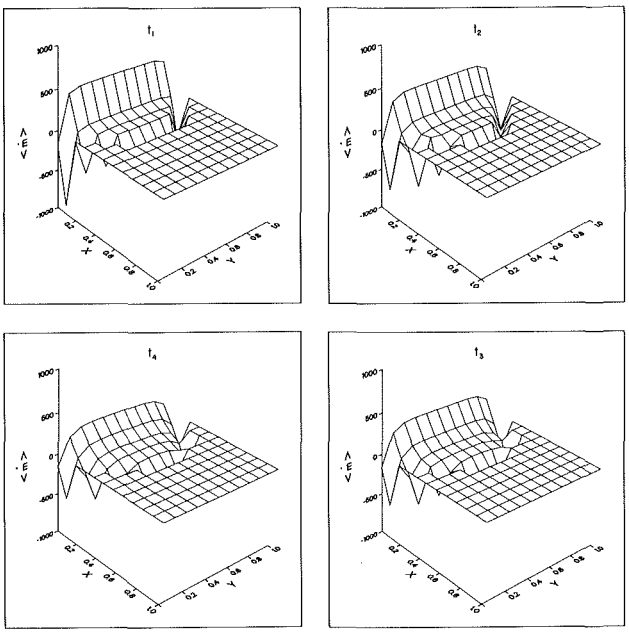


Fig. 11 Three-dimensional condensation and evaporation rate plots at four different times (Case II): $t_1 = 2.3 \times 10^{-3}$, $t_2 = 4.6 \times 10^{-3}$, $t_3 = 6.9 \times 10^{-3}$, $t_4 = 9.3 \times 10^{-3}$

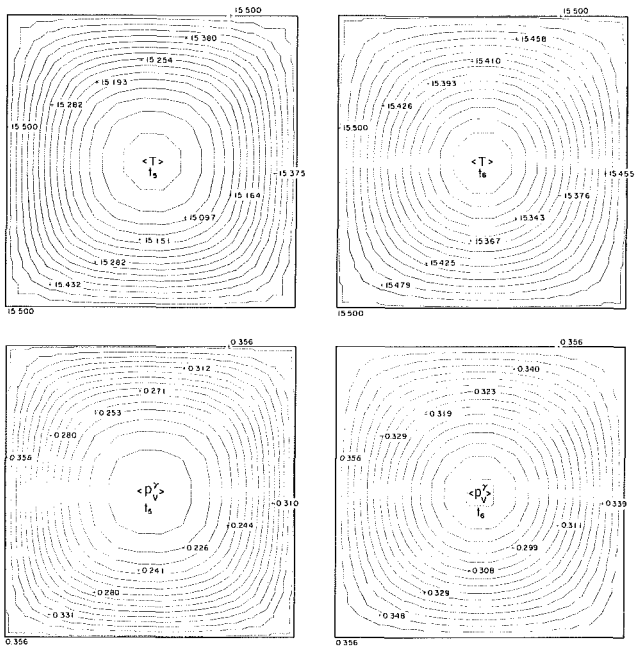


Fig. 13 Temperature and vapor pressure distributions approach toward steady state; presented at two different times: $t_5 = 6.9 \times 10^{-2}$, $t_6 = 0.21$

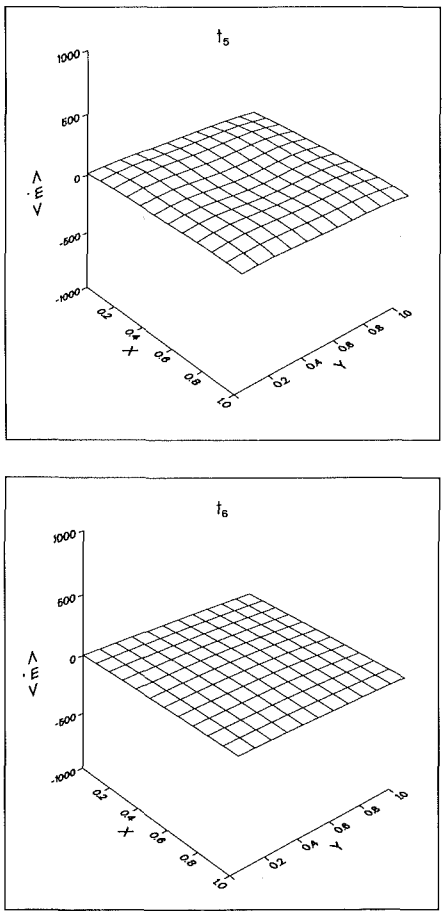


**Fig. 14 Three-dimensional condensation rate distribution approach toward steady state corresponding to Fig. 13**

$\Lambda\psi_s(\nabla S\cdot\nabla<T>)$, might be neglected for some practical problems.

II The term in the energy equation which accounts for the capillary pressure dependence on the temperature has a small effect on all of the pertinent variables. Therefore the term $\psi_T\Lambda(\nabla<T>\cdot\nabla<T>)$ in equation (3) can be neglected for some cases.

III The term related to the gravitational effects in the energy equation, $\Lambda\psi_g(\mathbf{g}\cdot\nabla<T>)$, can be neglected for most cases.

IV The term $\nabla\cdot(\psi_T\nabla<T>)$ (in the moisture transport equation) which accounts for the capillary pressure dependence on the temperature has a significant effect on all pertinent variables except the temperature field, where it has a small effect.

V The term $\nabla\cdot(\psi_s\nabla S)$, which represents the moisture flux, has a very important influence on all of the pertinent variables.

VI The term $\nabla\cdot(\psi_g\mathbf{g})$ in the moisture transport equation has a significant effect on all of the pertinent variables except the temperature field, where it has a small effect.

VII The variations in the total density $\rho$ and the mass fraction-averaged heat capacity $C_p$ do not alter the results significantly.

VIII Increasing the Lewis number decreases the liquid content and decreasing the Lewis number increases the liquid content at a given time and position.

IX The highest condensation regions seem to be located at the corners of the insulation slab.

Based on these results the following simplified version of equation (3) is recommended for analyzing the temperature distribution in a porous insulation material

$$\rho C_p\frac{\partial<T>}{\partial t}+<\dot{m}>=\nabla\cdot(k_{\text{eff}}\nabla<T>) \tag{32}$$

It should be noted that the results presented in this section were computed without making any simplifications. Further investigations on heat and mass transfer in porous insulation are recommended.

## References

1 Whitaker, S., "Simultaneous Heat, Mass and Momentum Transfer in Porous Media: A Theory of Drying," *Advances in Heat Transfer*, Vol. 13, Academic Press, New York, 1977.

2 Whitaker, S., "Advances in Theory of Fluid Motion in Porous Media," *Ind. Eng. Chem.*, Vol. 61, 1969, pp. 14-28.

3 Whitaker, S., "Toward a Diffusion Theory of Drying," *Ind. Eng. Chem. Fundam.*, Vol. 16, 1977, pp. 408-414.

4 Luikov, A. V., *Heat and Mass Transfer in Capillary-Porous Bodies*, Pergamon, Oxford, 1966.

5 Ceaglske, N. M., and Hougen, O. A., "Drying Granular Solids," *Ind. Eng. Chem.*, Vol. 29, 1937, pp. 805-813.

6 Eckert, E. R. G., and Faghri, M., "Moisture Migration in an Unsaturated Porous Medium," *IJHMT*, Vol. 23, 1980, pp. 1613-1623.

7 Burns, P. J., Chow, L. C., and Tien, C. L., "Convection in a Vertical Slot Filled With Porous Insulation," *IJHMT*, Vol. 20, 1977, pp. 919-926.

8 Langlais, C., Hyrien, M., and Karlsfeld, S., "Moisture Migration in Fibrous Insulating Material Under the Influence of a Thermal Gradient," in: *Moisture Migration in Buildings*, ASTM STP 779, 1982, pp. 191-206.